RSC Advances

PAPER

View Article Online
View Journal | View Issue

Cite this: *RSC Adv.*, 2017, **7**, 17612

Mn^{2+} doped $CdAl_2O_4$ phosphors with new structure and special fluorescence properties: experimental and theoretical analysis†

Weiguang Ran,[a] Lili Wang,[a] Qingzhi Liu,[a] Guangzeng Liu,[bc] Dan Qu,[a] Xiaohua Pan[a] and Jinsheng Shi*[a]

Received 8th February 2017
Accepted 14th March 2017

DOI: 10.1039/c7ra01623a

rsc.li/rsc-advances

Mn^{2+}-activated $CdAl_2O_4$ phosphors with the new structure of space group $R\bar{3}$ (no. 148) have been prepared by a high-temperature solid-state reaction and their luminescence properties have been investigated in detail. The reduction of Mn^{4+} to Mn^{2+} in air atmosphere has been observed in $CdAl_2O_4$ powders for the first time. The structural properties including the phase purity and structural parameters were analyzed through Rietveld analysis. The typical transitions of Mn^{2+} ions in emission and excitation spectra were observed both in $MnCO_3$ and MnO_2 prepared $CdAl_2O_4$:0.01Mn^{2+} phosphors, which means that the luminescent centers of Mn^{2+} ions were from the Mn^{4+} ions which were reduced. Meanwhile, the energy band structures of $CdAl_2O_4$ and $CdAl_2O_4$:Mn^{2+} were measured with an ultraviolet-visible diffuse reflection spectroscopy (UV-vis DRS), the electronic structures were calculated using the plane-wave density functional theory (DFT). The Mn^{2+} activated $CdAl_2O_4$:Mn^{2+} phosphor prepared in air atmosphere is a potential blue-green emitting phosphor.

1. Introduction

Phosphors prepared by the high-temperature solid-state reaction method have a high luminous intensity and good thermal stability.[1] Therefore, the high-temperature solid-state reaction is the most used method for the preparation of phosphors. When the luminescence centers need to be prepared at a lower valence state, people usually add reducing atmosphere such as H_2 into the reaction process. However, the introduction of reducing atmosphere not only improved the technological requirements and costs but also restricted the scope of applications. For example, when there exist some transition metal elements such as W, Mo, V, Cd, *etc.* which were easy to be reduced by reducing atmosphere in the host, there is no way to get low-valence luminescence centers. Therefore, reducing emitting ions to provide low-valence luminescence centers in an air atmosphere in the high-temperature solid-state reaction is still a research difficulty. At present, according to the reported literature, Eu^{3+} ions can be reduced to Eu^{2+} in an air atmosphere in some special crystal structure.[2–7] Peng[6] believe that it is closely related to the crystal structure and charge compensation.

Mn^{2+} ions as a common non-rare earth luminescence centers have been widely used.[8–10] The energy levels of Mn^{2+} ions are strongly affected by the lattice environment.[9] The luminescence properties have a great difference in different host lattices which made Mn^{2+} be an ideal non-rare earth luminescent center. However, people usually use the high-temperature solid-state reaction method in a reducing atmosphere to obtain Mn^{2+} ions activated phosphors. It greatly limits the scope of application of Mn^{2+} ions.

In this paper, we firstly synthesized $CdAl_2O_4$:Mn^{2+} phosphors by standard high-temperature solid-state reaction in an air atmosphere. The phosphors were characterized by X-ray diffraction (XRD), photoluminescence (PL) studies and Fourier transform infrared spectroscopy (FTIR). And the crystallographic parameters were refined through Rietveld analysis. The reduction activity of $CdAl_2O_4$ host was carefully studied by changing the manganese source. The geometry optimization and electronic structure calculations were performed using the Cambridge Serial Total Energy Package (CASTEP) code.[11] After analyzing the band structure and density of states, the emitting and energy transfer mechanism were detailly investigated. And the crystal field splitting parameter $10D_q$ was been calculated.

2. Synthesis and characterization

2.1 Sample synthesis

Samples of $CdAl_2O_4$ and $CdAl_2O_4$:Mn^{2+} were synthesized by the solid-state reaction method in an air atmosphere. The raw

[a]Qingdao Agricultural University, Qingdao 266109, People's Republic of China. E-mail: jsshiqn@aliyun.com

[b]State Key Laboratory of Crystal Materials, Shandong University, Jinan 250100, People's Republic of China

[c]College of Chemistry and Chemical Engineering, Qilu Normal University, Jinan, 250013, PR China

† Electronic supplementary information (ESI) available. CCDC 1536655. For ESI and crystallographic data in CIF or other electronic format see DOI: 10.1039/c7ra01623a

materials were CdO (99.99%), Al_2O_3 (99.99%), $MnCO_3$ (99.99%) and MnO_2 (99.99%). The starting materials were weighed according to the stoichiometric ratio and mixed with ethanol in agate container and ball milled with agate balls for 12 h. After milling, the mixed materials were dried in an oven at 60 °C for 24 h. The dried materials were put into the alumina crucible and calcined in a muffle furnace at 1200 °C for 3 h, and then the white powder phosphor was obtained. All samples were ground into a powder with an agate mortar and pestle for further analysis.

2.2 Experimental methods

The powder diffraction data of $CdAl_2O_4$ and $CdAl_2O_4$:0.03Mn^{2+} for Rietveld analysis were collected at room temperature with a Bruker D8 ADVANCE powder diffractometer (Cu Kα_1 radiation, $\lambda = 0.15406$ nm) and linear VANTEC detector. The step size of 2θ was 0.02°, and the counting time was 1 s per step. The Rietveld refinement was performed using the General Structure Analysis System (GSAS) program. Room-temperature photoluminescence emission (PL) and excitation (PLE) spectra were recorded using a Hitachi F-4600 spectrophotometer equipped with a 150 W xenon lamp as an excitation source. The luminescence decay curves were obtained from a FluoroLog-3-TCSPC. And the temperature-dependent luminescence properties were measured by a FluoroLog-3 spectrophotometer, which was combined with TAP-02 high-temperature fluorescence controller (Orient KOJI, Tianjin). With the crystal structure data, which were obtained by Rietveld refinement, DFT calculations on the trigonal $CdAl_2O_4$ host and the Mn^{2+} doped samples were carried out by using the CASTEP code.[11]

3. Results and discussion

3.1 Phase identification and morphology

The space group of $CdAl_2O_4$ in this paper is $R\bar{3}$, which is different from the reported $CdAl_2O_4$ spinel structure with space group $Fd\bar{3}ms$.[12] The structure of $CdAl_2O_4$ in this paper has the same structure with Zn_2SiO_4, both of them have the similar crystal structure with β-Si_3N_4.[13] Therefore, the structure model of $CdAl_2O_4$ in this paper is selected on Zn_2SiO_4. As shown in Fig. 1, compared with Zn_2SiO_4 ($R\bar{3}$ PDF# 37-1485), the prepared $CdAl_2O_4$ powder with space group $R\bar{3}$ (PDF# 34-0071) has the similar position and intensity of diffraction peaks. The XRD pattern of the $CdAl_2O_4$ sample was defined by a Rietveld refinement implemented with the Zn_2SiO_4 (ICSD #67235) $R\bar{3}$ (148) structure model. The observed, calculated, background and the difference patterns of the XRD refinement of $CdAl_2O_4$ are shown in Fig. 2. The final refinement converged with weighted profiles of $R_p = 6.03\%$, $R_{wp} = 8.41\%$ and $\chi^2 = 2.624$, which illustrates there is no detectable impurity phase observed in this obtained sample. As the crystallographic data of $CdAl_2O_4$ shown in Table 1, this compound exhibits a trigonal crystal system with the space group $R\bar{3}$ (no. 148), $Z = 18$, and the cell parameter is $a = b = 14.2210$ Å, $c = 9.5733$ Å, $V = 1676.69$ Å^3. As shown in Fig. 2, the refinements were stable and gave low R-factors. And the refined structural parameters of $CdAl_2O_4$ are listed in Table 1. The optimized crystal structural parameters of $CdAl_2O_4$ after geometry optimization are listed in Table S1.† It can be seen that the results of Rietveld refinement are very similar to those of structure calculated after geometry

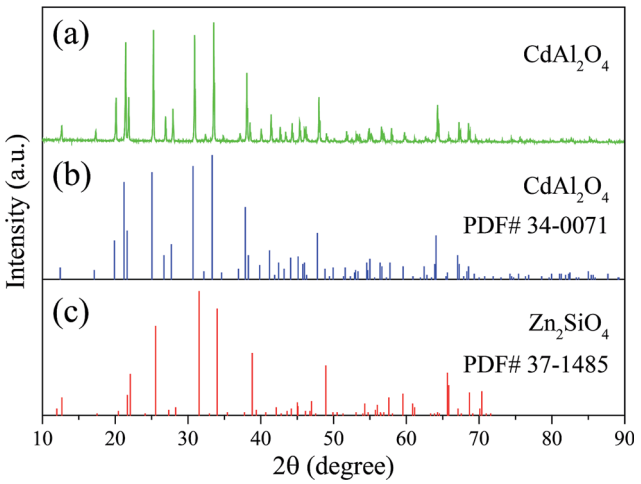

Fig. 1 XRD patterns of (a) $CdAl_2O_4$ samples and standard card of (b) $CdAl_2O_4$ and (c) Zn_2SiO_4 powders.

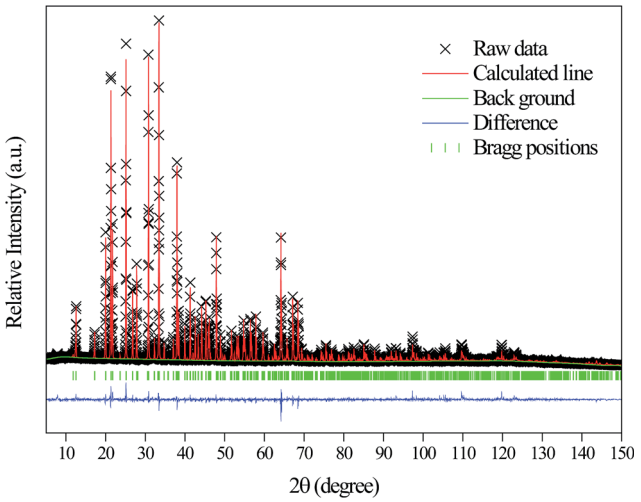

Fig. 2 Rietveld analysis patterns of X-ray powder diffraction data of $CdAl_2O_4$ phosphors.

Table 1 Refined structural parameters of $CdAl_2O_4$ obtained from the Rietveld refinement[a]

Element symbol	Mult. Wyck.	x/a	y/b	z/c	U (Å^2)
Cd1	18f	0.2061	0.1835	0.2456	0.0261
Al1	18f	0.2072	0.1977	0.5818	0.0260
Al2	18f	0.2166	0.1970	0.9170	0.0229
O1	18f	0.3425	0.3469	0.2456	0.0147
O2	18f	0.2201	0.1110	0.0494	0.0221
O3	18f	0.2172	0.1210	0.4467	0.027
O4	18f	0.1935	0.1391	0.7514	0.0234

[a] $a = b = 14.2210$, $c = 9.5733$, $\alpha = \beta = 90°$, $\gamma = 120°$, $V = 1676.69$ Å^3, space group $R\bar{3}$, $R_{wp} = 8.41\%$, $R_{exp} = 6.03\%$, $\chi^2 = 2.624$.

optimization with CASTEP program. From the first principles calculation, to investigate the reasonableness of the $CdAl_2O_4$ structure, the phonon spectrum of $CdAl_2O_4$ was calculated after geometry optimization (see Fig. S1†). The absence of any imaginary frequency phonon modes proves the dynamical stability of the $CdAl_2O_4$ with $R\bar{3}$ structure.

In the crystal structure of $CdAl_2O_4$ shown in Fig. 3, the Cd atoms occupy the 18f site coordinated by four O atoms to form CdO_4 tetrahedron. Al atoms are occupied the 18f site in the center of AlO_4 tetrahedron.

3.2 Luminescence properties and valence analysis of Mn ions

Fig. 4 shows the manganese source dependent PL and PLE spectra of $Cd_{0.99}Mn_{0.01}Al_2O_4$ phosphors. As seen from the PL and PLE spectra, their shape and intensity of fluorescence spectrum are very similar. The emission spectra just have one single emission peak at about 495 nm, which is consistent with the traditional Mn^{2+} emission.[14–17] This indicates that whether using $MnCO_3$ or MnO_2, the phosphors prepared by high-temperature solid phase reaction method in air atmosphere have typical characteristic peaks of Mn^{2+} ions. $CdAl_2O_4$:0.01-Mn^{2+} fluorescent material has a strong characteristic emission

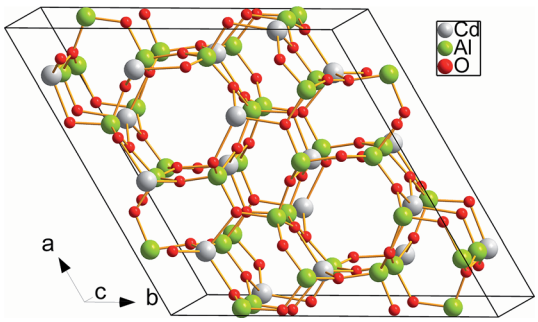

Fig. 3 Crystal structure of $CdAl_2O_4$ by Rietveld analysis.

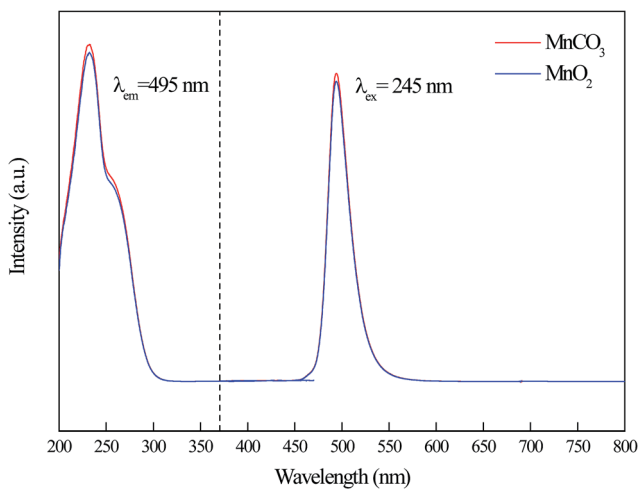

Fig. 4 Excitation and emission spectra of $Cd_{0.99}Mn_{0.01}Al_2O_4$ phosphors from different raw materials.

of Mn^{2+} ions when $MnCO_3$ was added as manganese source. This indicates that Mn^{2+} ions were not oxidized in an air atmosphere in high-temperature solid-state reaction. In addition, we further investigated the luminescent properties of $CdAl_2O_4$:0.01Mn^{2+} phosphor with MnO_2 as manganese source. Although the manganese source has only Mn^{4+} ions, the $CdAl_2O_4$:0.01Mn^{2+} phosphor still exhibits a strong characteristic emission of Mn^{2+} ions. It means that the luminescent centers of Mn^{2+} ions come from the Mn^{4+} ions which were reduced at high temperatures. Compared with the emission intensity of $Cd_{0.99}Mn_{0.01}Al_2O_4$ phosphor prepared by $MnCO_3$, the emission intensity prepared by MnO_2 was only reduced 2.6%. This could be a result of experimental errors. And there is a very strong reduction activity in the $CdAl_2O_4$ host. The Mn^{4+} ions were reduced almost entirely to Mn^{2+} in air atmosphere by a high-temperature solid-state reaction.

The XPS test was employed to analyze the valence of Mn in $CdAl_2O_4$:Mn phosphors. The $CdAl_2O_4$:0.015Mn^{2+} phosphor which was prepared in air atmosphere by MnO_2 was selected. Fig. S2(a)† displays the survey scan of $CdAl_2O_4$:Mn phosphors, where the principal peaks are corresponding to cadmium (Cd 3d), aluminum (Al 2s, Al 2p), carbon (C 1s) and oxygen (O 1s). The binding energy for the Mn 3s orbital of Mn^{2+} is not evident due to the low doping concentration. Therefore, we can't use the gap of two peaks in Mn 3s orbital to determine the valence of Mn. The XPS spectrum of the phosphor in $2p_{3/2}$ and $2p_{1/2}$ region of Mn is shown in Fig. S2(b).† The binding energy of 641 and 653 eV indicates that the Mn ion has +2 oxidation state. However, a principal peak at about 651 eV which belong to the binding energies of Cd $3p_{1/2}$ affects the judgment of the oxidation state of Mn. Therefore, the valence of the Mn is not clear from XPS, and it should be considered from the viewpoint of the fluorescence properties. As can be seen from Fig. 5, since $CdAl_2O_4$:Mn^{2+} fluorescent material exists only broadband emission at about 495 nm, which is consistent with Mn^{2+} ions fluorescence characteristics.[18–20] And there is no typical linear emission peak of Mn^{4+} in the red-light region. Therefore, the valence of Mn element in $CdAl_2O_4$:0.015Mn^{2+} sample prepared by using MnO_2 in air atmosphere is Mn^{2+}.

Fig. 5(a) shows the excitation spectrum of the pure $CdAl_2O_4$ sample monitored at about 395 nm. The asymmetric broadband at about 200–260 nm (40 000–38 460 cm^{-1}) was decomposed into two components (220.8 nm and 236.9 nm) by Gaussian fitting. Fig. 5(b) shows the excitation spectrum of the $CdAl_2O_4$:0.01Mn^{2+} sample monitored at about 495 nm. Compared with Fig. 5(a), the excitation band at about 264.5 nm (37 810.51 cm^{-1}) can be assigned to the O–Mn charge transfer band of $CdAl_2O_4$:0.01Mn^{2+} phosphor. The Fig. 5(c) shows an enlarged view in the 330–470 nm range. The excitation spectrum presents many narrow transitions, associated to $^6A_1(^6S)$–$^4E_g(^4D)$ (354 nm), $^6A_1(^6S)$–^4E_g,$^4A_{1g}(^4G)$ (426 nm), $^6A_1(^6S)$–$^4T_{2g}(^4G)$ (436 nm), $^6A_1(^6S)$–$^4T_{1g}(^4G)$ (460 nm) electronic transitions. This indicates that although the Mn^{4+} were used as Mn source, it was eventually reduced to Mn^{2+} ions in $CdAl_2O_4$ phosphors *via* a high-temperature solid-state reaction method in an air atmosphere. Fig. 5(d) shows the emission spectrum of $CdAl_2O_4$:0.01Mn^{2+} phosphor. The maximum of the emission is at about 495 nm,

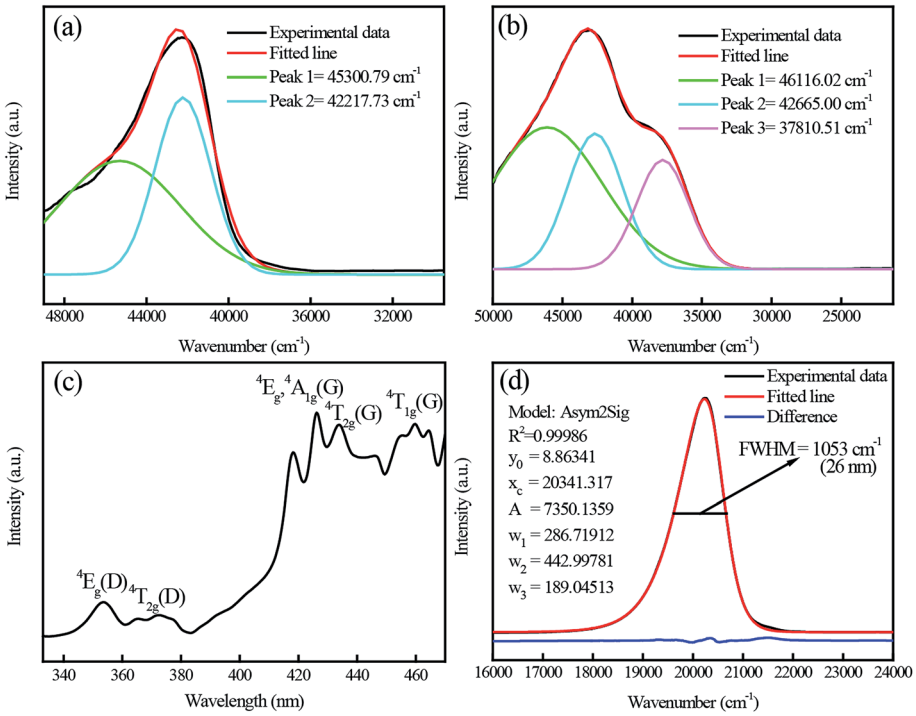

Fig. 5 Excitation and emission spectra of as prepared $CdAl_2O_4$ and $CdAl_2O_4$:0.01Mn^{2+} sample.

with an FWHM of only 1053 cm^{-1} (26 nm). Moreover, the emission spectrum shows asymmetrical double sigmoidal (Asym2sig) fit (red) with $R^2 = 0.99986$. The Asym2sig function is distributed as follows:

$$y = y_0 + \frac{1}{1+e^{\left(-\frac{x-x_c+w_1/2}{w_2}\right)}}\left[1 - \frac{1}{1+e^{\left(-\frac{x-x_c-w_1/2}{w_3}\right)}}\right]$$

where x_c is the peak position and w_1, w_2 and w_3 are related to the width and asymmetry of the peak distribution.[21]

Mn^{2+} doping Zn_2SiO_4 have been extensively studied in the reported literature.[19,22–24] Excitation and emission spectra of as prepared Zn_2SiO_4:0.01Mn^{2+} phosphor are shown in Fig. S3.† It can be seen that the excitation and emission spectra of $CdAl_2O_4$:Mn^{2+} are very similar to Zn_2SiO_4:Mn^{2+} phosphor. The typical excitation and emission peaks of Mn^{2+} were observed. There are three broad excitation bands and several sharp excitation peaks which positions are very close to $CdAl_2O_4$:Mn^{2+} in the excitation spectra. And both of them have only one emission band which was explained by the asymmetrical double sigmoidal (Asym2sig) function.

From Fig. 6, PL and PLE spectra of $CdAl_2O_4$, $CdAl_2O_4$:0.0001Mn^{2+} and $CdAl_2O_4$:0.01Mn^{2+} phosphors are presented in an immediate contrast. From Fig. 6(a), pure $CdAl_2O_4$ phosphor exhibits a strong blue-violet emission band with a maximum at about 395 nm. When monitoring at 395 nm, the excitation spectrum of $CdAl_2O_4$ exhibits a broad band in the range of 200–250 nm with the main peak at about 230 nm. As shown in Fig. 6(b), under the excitation of 230 nm, two broad emission bands centered at 395 nm and 495 nm were observed in $CdAl_2O_4$:0.0001Mn^{2+} phosphor. The new emission band centered at 495 nm is attributed to the typical $^4T_{1g}(4G)$–$^6A_{1g}(6S)$ transition of the Mn^{2+} ions. Fig. 6(c) shows the PL excitation and emission spectra of $CdAl_2O_4$:0.01Mn^{2+} phosphor. As depicted in Fig. 6(c), the excitation spectrum monitored at 495 nm of $CdAl_2O_4$:0.01Mn^{2+} sample primarily contains two broad bands centered at 230 nm and 260 nm. As for the emission spectrum, although the intensity of the blue emission is reduced compared to the pure $CdAl_2O_4$ phosphor, but the emission intensity of Mn^{2+} ions increased as large as several hundred times. The emission spectrum of $CdAl_2O_4$ host and excitation spectrum of $CdAl_2O_4$:0.01Mn^{2+} phosphor were shown in an immediate contrast in Fig. 6(d), the $CdAl_2O_4$ emission band

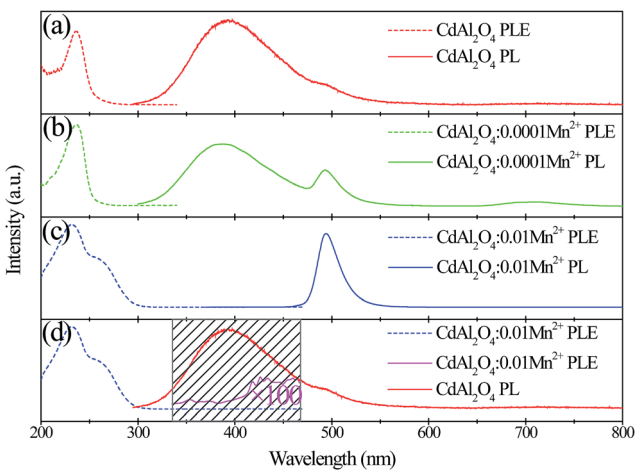

Fig. 6 PL and PLE spectra of $CdAl_2O_4$ and $CdAl_2O_4$:0.01Mn^{2+} phosphors.

overlaps with the Mn^{2+} excitation peaks in the range 330–460 nm, and the energy transfer was expected to occur from $CdAl_2O_4$ host to Mn^{2+} ions.

Fig. 7 shows the dependence of Mn^{2+} fluorescence intensity on concentrations. From the emission spectra, it can be seen that Mn^{2+} ions emission intensity of the blue-green emission band increase until the maximum x at 0.015. When the concentration of Mn^{2+} is further increased above 0.015, the emission intensity begins to decrease which can be explained by the appearance of concentration quenching effect at high Mn^{2+} content. The PL excitation spectra of the samples with different concentrations of Mn^{2+} ions were monitored at the emission wavelength of 495 nm. However, the optimal doping concentration of 230 nm excitation band is 0.015 while 264 nm excitation band and d–d transition bands are 0.02. This indicates that the origins of excitation bands are different.

To further investigate the characteristics of $CdAl_2O_4$:Mn^{2+} phosphor, the thermal quenching behavior was measured. Fig. S4† depicts the temperature-dependent emission spectra. As can be seen from the picture, with the increase of environment temperature, the emission intensity gradually decreased. The emission intensity of $CdAl_2O_4$:Mn^{2+} phosphor has reduced by about 50% when the temperature exceeds 100 °C. This indicates that $CdAl_2O_4$:Mn^{2+} phosphors are more suitable for low-temperature environment application.

Furthermore, the decay curves of $CdAl_2O_4$:0.015Mn^{2+} phosphor ($\lambda_{ex} = 266$ nm and $\lambda_{em} = 495$ nm) at room temperature was shown in Fig. S5.† The red curves are a fit of the experimental data to a first order exponential decay equation which indicates that there is one kind of luminescence center homogeneously distributed in the phosphor. This means that Mn^{2+} occupies the Cd^{2+} 18f sites. The decay curves were well fitted by a first-order exponential decay equation

$$I_{(t)} = I_{(0)} \exp(-t/\tau)$$

where $I_{(0)}$ is the initial luminescence intensity, $I_{(t)}$ is the luminescence intensity at time t, t is the time, and τ is the decay constant for the exponential component. The fluorescence lifetime of the optimized blue-green emitting $CdAl_2O_4$:0.015-Mn^{2+} phosphor is 12.1 ms.

Fig. S6† exhibits the variation of the Commission International de L'Eclairage (CIE) chromaticity coordinates of the $CdAl_2O_4$, $CdAl_2O_4$:0.0001Mn^{2+} and $CdAl_2O_4$:0.015Mn^{2+} phosphors under excitation at 230 nm. The pure $CdAl_2O_4$ host emits blue-violet light with CIE coordinates of (0.1674, 0.1053). When the concentration of Mn^{2+} is increased to 0.015, a blue-green light can be obtained with CIE coordinates of (0.0704, 0.4800). The results indicate that the emission light can be modulated from blue-violet to blue-green with the increasing doping content of Mn^{2+} ions.

3.3 Sites occupation and structural analysis

It is well known that Mn^{2+} ions with similar ionic radius and charge could enter into the lattice by substituting Cd^{2+} sites. In order to further investigate the phase formation depending on the Mn^{2+} substitution of $CdAl_2O_4$ phosphors, XRD patterns for the selected samples with 3% substitution amount of Cd for $CdAl_2O_4$ were shown in Fig. 8.

As shown in Fig. 8, all peaks were indexed by trigonal cell $R\bar{3}$ (no. 148) with parameters close to $CdAl_2O_4$ crystal structures. The calculated and observed patterns fit fairly well, and no impurity phases were detected. The refined structural parameters of $CdAl_2O_4$:0.03Mn^{2+} are listed in Table S2.† With Mn^{2+} ions occupied Cd (18f) sites, the cell volume of compound is smaller than cell volume of $CdAl_2O_4$, which is in accordance with smaller value of ion radii (IR) of Mn^{2+} (CN = 4, IR = 0.66 Å) in comparison with ion radii (IR) of Cd^{2+} (CN = 4, IR = 0.78 Å).

The Fourier transform infrared (FTIR) investigation was carried out to study the crystal structure. Fig. 9(a) and (b) shows the FTIR spectra of the as-prepared $CdAl_2O_4$ phosphor by high-temperature solid-state reaction method. The bands in the range 540–1000 cm^{-1} can be attributed to the asymmetric stretching vibrations of [AlO_4^{5-}] tetrahedral units as described in Fig. 9(a). And the bands in range 540–400 cm^{-1} was assigned

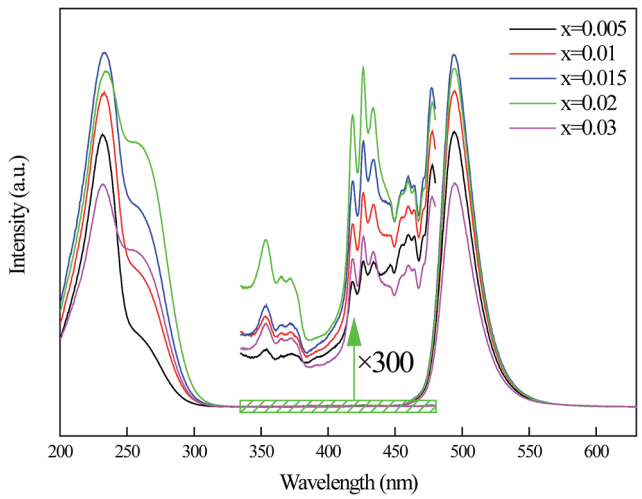

Fig. 7 Variation of excitation and emission spectra for $CdAl_2O_4$:xMn^{2+} samples.

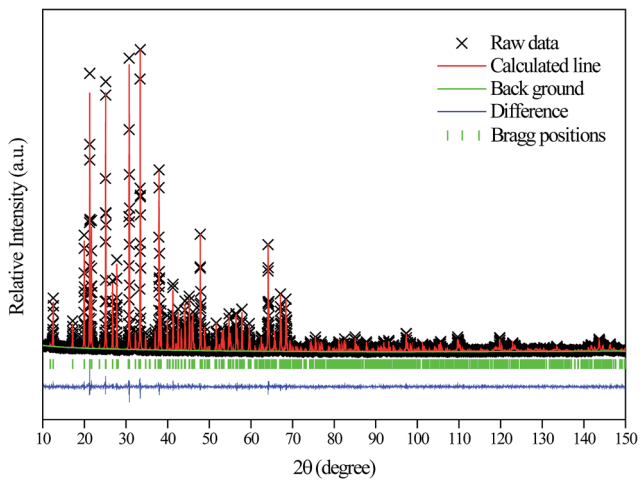

Fig. 8 Rietveld analysis patterns of X-ray powder diffraction data of $CdAl_2O_4$:0.03Mn^{2+} phosphors.

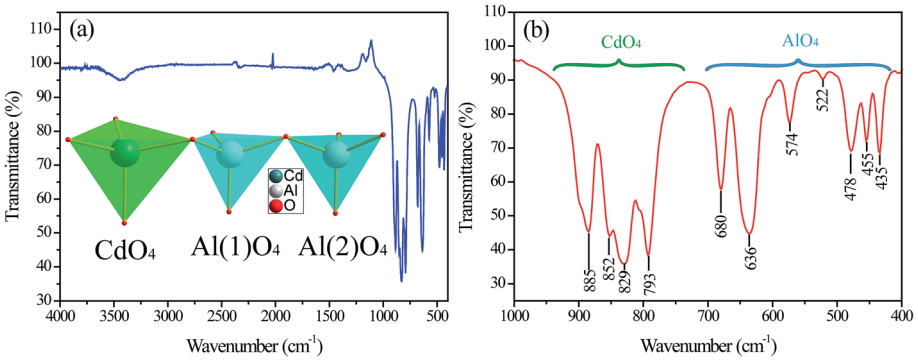

Fig. 9 FTIR spectrum of $CdAl_2O_4$ crystals. (a) Full range 4000–400 cm^{-1} and (b) 1000–400 cm^{-1}.

to asymmetric stretching vibrations of Cd–O bands of $[CdO_4^{6-}]$ tetrahedral units as shown in Fig. 9(a).

3.4 Measurement of optical bandgap

Fig. 10 gives the UV-vis absorption spectra of $CdAl_2O_4$ and $CdAl_2O_4$:0.015Mn^{2+} phosphors. It is observed that all of the samples have strong absorption of UV light. With the introduction of Mn^{2+}, the abstraction band edge of the $CdAl_2O_4$:0.01Mn^{2+} phosphor redshifts obviously, which indicates that the introduced Mn^{2+} ions provide a new absorption band. Simultaneously, the optical band gap of $CdAl_2O_4$ phosphor has been shrinking significantly. The correlation between the absorption coefficient of semiconductor oxides and optical band gap E_{gap} can be determined by the following equation:[25,26]

$$F(R_\infty)h\nu \propto (h\nu - E_{gap})^n$$

$$F(R_\infty) = \frac{(1-R_\infty)^2}{2R_\infty}$$

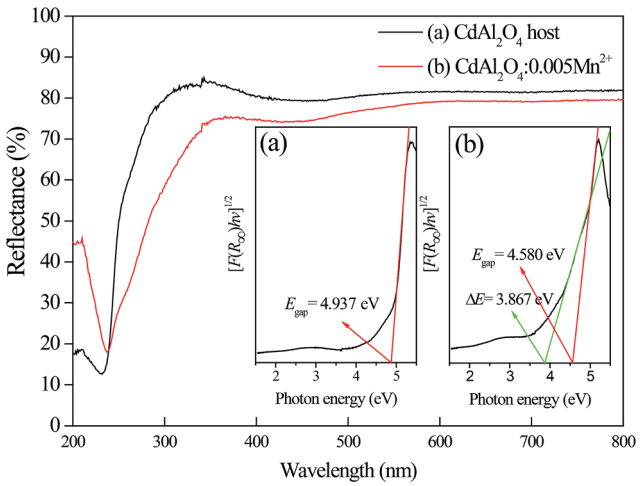

Fig. 10 Diffuse reflectance spectrum of $CdAl_2O_4$ and $CdAl_2O_4$:0.015Mn^{2+} phosphors. The inset shows the corresponding Tauc plots curves and determination of the optical band gaps: (a) $CdAl_2O_4$ and (b) $CdAl_2O_4$:0.015Mn^{2+}.

where R_∞ is the reflectivity of the sample, h is the Plank constant, ν is the photon energy, and n is determined by the transition type (n = 1/2, 2, 3/2 or 3 for allowed direct, allowed indirect, forbidden direct and forbidden indirect electronic transitions, respectively).

According to the calculation results of band structures from density functional theory (DFT) below (Fig. 11), $CdAl_2O_4$ and $CdAl_2O_4$:Mn^{2+} has been confirmed to be allowed indirect band gap materials, therefore, n = 2:

$$h\nu - E_{gap} \propto (F(R_\infty)h\nu)^{1/2}$$

Based on the results, we can get the Tauc-plots of samples as shown in the inset of Fig. 10. As can be seen from the picture, with the introduction of Mn^{2+} ions, the Mn^{2+} doped band gap of $CdAl_2O_4$ was shrinking from 4.937 eV into 4.580 eV. The absorption boundary of Mn^{2+} ions in $CdAl_2O_4$ host is 3.867 eV.

3.5 First principles calculation

We calculated the crystal structure optimization and electronic structure of the $CdAl_2O_4$ and $CdAl_2O_4$:Mn^{2+} phosphors by the first-principles method. The optimized crystal structural parameters of $CdAl_2O_4$ after geometry optimization are listed in Table S1.† The optimized crystal structural parameters were very close to the results of Rietveld refinements. To further verify the reasonableness of the structure we calculate the phonon spectrum of $CdAl_2O_4$ after geometry optimization (see Fig. S1†). As can be seen from the Fig. S1,† the absence of any imaginary frequency phonon modes proves the dynamical stability of the $CdAl_2O_4$ with $R\bar{3}$ structure.

The calculated band structures in Fig. 11 revealed that $CdAl_2O_4$:Mn^{2+} is indirect band gap materials (G point to Q point). It is well known that the CASTEP simulation results tend to underestimate the band-gap energies of the semiconductor materials due to the limited dimension of the atomic cluster. Therefore, a scissors operator of 2.235 eV was introduced to widen the gap to consistent with the measured optical band gap value (4.937 eV) of $CdAl_2O_4$:Mn^{2+} phosphors, which agrees well with the absorption edge (250 nm) of the $CdAl_2O_4$ without Mn^{2+} doping.

According to the orbital population analysis of $CdAl_2O_4$ phosphor from Fig. 12 (left), the top of the valence band is

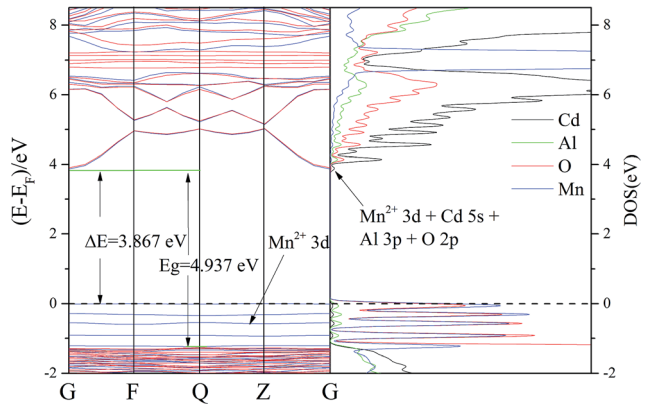

Fig. 11 Band structure (left) and PDOS (right) of $CdAl_2O_4$:Mn^{2+} phosphors.

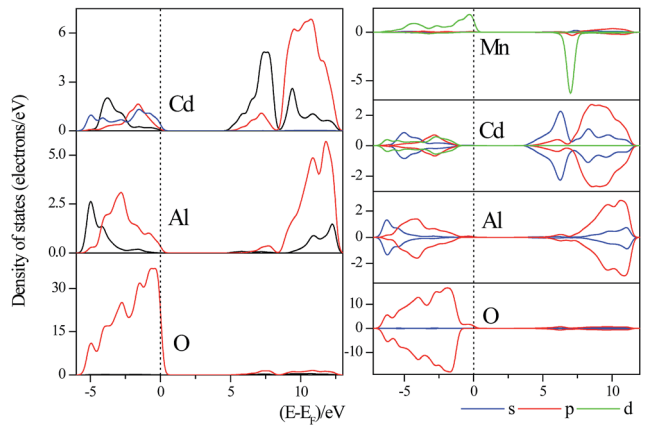

Fig. 12 Partial DOSs of ideal $CdAl_2O_4$ (left) and $CdAl_2O_4$:Mn^{2+} (right) near the Fermi energy level. The Fermi energy is at zero.

dominated by the 2p orbitals of O atoms, the interband transition could be ascribed to the charge transfer from the O-2p to Cd-4d orbitals, which basically corresponds to the excitation energy of $CdAl_2O_4$ host in Fig. 5(a). From Fig. 12 (right) it can be seen that with the Mn^{2+} doping, the valence band is dominated by the 2p orbitals of O and 3d orbitals of Mn^{2+} ions, the interband transition could be ascribed to the charge transfer from the O-2p to Cd-4d orbitals and from the Mn-3d to Mn-3d orbitals, which basically corresponds to the excitation energy of $CdAl_2O_4$:0.015Mn^{2+} sample in Fig. 5(b).

Herein, by combining the excitation spectra of $CdAl_2O_4$:Mn^{2+} phosphors with the parity selection rules and Sugano–Tanabe energy diagram, a detailed spectral analysis and the fitting of crystal field parameters were performed. The sharp bands in the excitation spectra centered at 353 nm (2.83×10^4 cm^{-1}) and 426 nm (2.35×10^4 cm^{-1}) can be attributed to the parity forbidden transitions of $^4E_g(^4D) \rightarrow {}^6A_{1g}(^6S)$ and $^4E_g(^4G) \rightarrow {}^6A_{1g}(^6S)$ which are D_q-independent, respectively. The vertical dashed line indicates the appropriate value of Δ/B (4.98), and the horizontal ones are used to compare the peaks of the absorption of Mn^{2+} to the energy states in the Tanabe–Sugano diagram in Fig. 13. With the assignment of $17B + 5C = E(^4E_g(^4D))$ and $10B + 5C = E(^4E_g(^4G))$ the Racah parameters B and C for the tetrahedrally coordinated Mn^{2+} were calculated to be $B = 692.8$ cm^{-1}, $C = 3307$ cm^{-1}, and $\gamma = C/B = 4.77$. $\Delta/B = 4.98$ and $\Delta_o = 3450$ cm^{-1}. Since Mn^{2+} occupies the four-coordinated Cd^{2+} lattice in $CdAl_2O_4$, it is reported that Δ_T for tetrahedral complexes is approximately 4/9 of Δ_o for an octahedral complex. Therefore, the crystal field splitting parameter $10D_q = \Delta_T = 4/9\Delta_o = 1533$ cm^{-1} of Mn^{2+} in $CdAl_2O_4$ were derived.

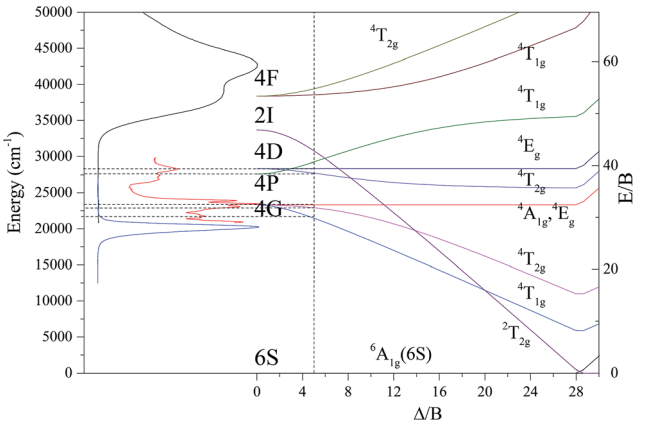

Fig. 13 The excitation and emission spectra of $CdAl_2O_4$:0.02Mn^{2+} phosphors associated with the Tanabe–Sugano diagram.

4. Conclusion

In conclusion, the structure of new $CdAl_2O_4$ material with space group $R\bar{3}$ was determined. Mn^{2+} ions activated blue-green emitting phosphors $CdAl_2O_4$:xMn^{2+} have also been successfully obtained by a conventional high-temperature solid-state reaction method in an air atmosphere. The typical transitions of Mn^{2+} ions in emission and excitation spectra were observed both in $MnCO_3$ and MnO_2 prepared $CdAl_2O_4$:0.01Mn^{2+} phosphors. $CdAl_2O_4$:Mn^{2+} fluorescent materials have a strong characteristic emission of Mn^{2+} ions when $MnCO_3$ was added as manganese source. That is to say in the $CdAl_2O_4$ host, Mn^{2+} ions were not oxidized in the air atmosphere in high-temperature solid-state reaction. For MnO_2 as manganese source, the $CdAl_2O_4$:Mn^{2+} phosphors still exhibit a strong characteristic emission of Mn^{2+} ions. This indicates that the luminescent centers of Mn^{2+} ions come from the Mn^{4+} ions which were reduced at high temperatures. The crystal field splitting parameter $10D_q$ was estimated to be 1533 cm^{-1}. Although the valence of manganese source was different, their shape and intensities of emission and excitation spectra were very similar. When excited by ultraviolet light, the Mn^{2+} ions occupied Cd sites emitting strong blue-green luminescence.

Acknowledgements

This work was supported by Science and Technology Development Plan of Shandong Province, China (2014GNC110013) and National Natural Science Foundation for Young (No. 2130696).

References

1 Y. Pan, M. Wu and Q. Su, Comparative investigation on synthesis and photoluminescence of YAG: Ce phosphor, *Mater. Sci. Eng., B*, 2004, **106**, 251–256.

2 H. Xie, J. Lu, Y. Guan, Y. Huang, D. Wei and H. J. Seo, Abnormal Reduction, $Eu^{3+} \rightarrow Eu^{2+}$, and Defect Centers in Eu^{3+}-Doped Pollucite, $CsAlSi_2O_6$, Prepared in an Oxidizing Atmosphere, *Inorg. Chem.*, 2014, **53**, 827–834.

3 J.-C. Zhang, Y.-Z. Long, H.-D. Zhang, B. Sun, W.-P. Han and X.-Y. Sun, Eu^{2+}/Eu^{3+}-emission-ratio-tunable $CaZr(PO_4)_2$:Eu phosphors synthesized in air atmosphere for potential white light-emitting deep UV LEDs, *J. Mater. Chem. C*, 2014, **2**, 312–318.

4 M. Peng, Z. Pei, G. Hong and Q. Su, Study on the reduction of $Eu^{3+} \rightarrow Eu^{2+}$ in $Sr4Al_{14}O_{25}$: Eu prepared in air atmosphere, *Chem. Phys. Lett.*, 2003, **371**, 1–6.

5 M. Peng and G. Hong, Reduction from Eu^{3+} to Eu^{2+} in $BaAl_2O_4$: Eu phosphor prepared in an oxidizing atmosphere and luminescent properties of $BaAl_2O_4$: Eu, *J. Lumin.*, 2007, **127**, 735–740.

6 M. Peng, Z. Pei, G. Hong and Q. Su, The reduction of Eu^{3+} to Eu^{2+} in $BaMgSiO_4$:Eu prepared in air and the luminescence of $BaMgSiO_4$:Eu^{2+} phosphor, *J. Mater. Chem.*, 2003, **13**, 1202–1205.

7 Z. Pei, Q. Zeng and Q. Su, The application and a substitution defect model for $Eu^{3+} \rightarrow Eu^{2+}$ reduction in non-reducing atmospheres in borates containing BO_4 anion groups, *J. Phys. Chem. Solids*, 2000, **61**, 9–12.

8 W. Liu, Q. Lin, H. Li, K. Wu, I. Robel, J. M. Pietryga and V. I. Klimov, Mn^{2+}-Doped Lead Halide Perovskite Nanocrystals with Dual-Color Emission Controlled by Halide Content, *J. Am. Chem. Soc.*, 2016, **138**, 14954–14961.

9 L. Wang, L. Tan, T. Hou and J. Shi, Investigation of change regularity of energy states of Mn^{2+} in halides, *J. Lumin.*, 2013, **134**, 319–324.

10 W.-R. Liu, C.-H. Huang, C.-W. Yeh, Y.-C. Chiu, Y.-T. Yeh and R.-S. Liu, Single-phased white-light-emitting $KCaGd(PO_4)_2$: Eu^{2+},Tb^{3+},Mn^{2+} phosphors for LED applications, *RSC Adv.*, 2013, **3**, 9023–9028.

11 M. D. Segall, J. D. L. Philip, M. J. Probert, C. J. Pickard, P. J. Hasnip, S. J. Clark and M. C. Payne, First-principles simulation: ideas, illustrations and the CASTEP code, *J. Phys.: Condens. Matter*, 2002, **14**, 2717.

12 H. Hahn, G. Frank, W. Klingler, A. D. Störger and G. Störger, Untersuchungen über ternäre chalkogenide. VI. Über Ternäre chalkogenide des aluminiums, galliums und indiums mit zink, cadmium und Quecksilber, *Z. Anorg. Allg. Chem.*, 1955, **279**, 241–270.

13 G. A. Slack and I. C. Huseby, Thermal Grüneisen parameters of $CdAl_2O_4$, β–Si_3N_4, and other phenacite-type compounds, *J. Appl. Phys.*, 1982, **53**, 6817–6822.

14 Y. F. Liu, X. Zhang, Z. D. Hao, Y. S. Luo, X. J. Wang and J. H. Zhang, Generating yellow and red emissions by co-doping Mn^{2+} to substitute for Ca^{2+} and Sc^{3+} sites in $Ca_3Sc_2Si_3O_{12}$:Ce^{3+} green emitting phosphor for white LED applications, *J. Mater. Chem.*, 2011, **21**, 16379–16384.

15 L. Wang, Z. Hou, Z. Quan, H. Lian, P. Yang and J. Lin, Preparation and luminescence properties of Mn^{2+}-doped $ZnGa_2O_4$ nanofibers *via* electrospinning process, *Mater. Res. Bull.*, 2009, **44**, 1978–1983.

16 S. G. Kim, S. H. Lee, N. H. Park, H. L. Park, K. W. Min, S. I. Mho, T. W. Kim and Y. H. Hwang, Mn^{2+} site behaviors in $Cd_xZn_{1-x}Ga_2O_4$ and $Sr_xBa_{1-x}Al_{12}O_{19}$ green phosphors, *Solid State Commun.*, 1999, **110**, 515–518.

17 M. Shang, G. Li, D. Yang, X. Kang, C. Peng, Z. Cheng and J. Lin, $(Zn, Mg)_2GeO_4$:Mn^{2+} submicrorods as promising green phosphors for field emission displays: hydrothermal synthesis and luminescence properties, *Dalton Trans.*, 2011, **40**, 9379–9387.

18 Z. Wang, L. Feng, J. Zhang, Z. Ci, Z. Zhang and Y. Wang, Nonequivalent Substitution and Charge-Induced Emitter-Migration Design of Tuning Spectral and Duration Properties of $NaCa_2GeO_4F$: Mn^{2+} Persistent Luminescent Phosphor, *Inorg. Chem.*, 2016, **55**, 7988–7996.

19 R. Ye, G. Jia, D. Deng, Y. Hua, Z. Cui, S. Zhao, L. Huang, H. Wang, C. Li and S. Xu, Controllable Synthesis and Tunable Colors of α- and β-Zn_2SiO_4:Mn^{2+} Nanocrystals for UV and Blue Chip Excited White LEDs, *J. Phys. Chem. C*, 2011, **115**, 10851–10858.

20 L. Hu, Q. Wang, X. Wang, Y. Li, Y. Wang and X. Peng, Photoluminescence and cathodoluminescence properties of Na_2MgGeO_4:Mn^{2+} green phosphors, *RSC Adv.*, 2015, **5**, 104708–104714.

21 L. Changshi, Prediction of the photoluminescence of $In_{0.53}Ga_{0.47}As$/InP irradiated by 1 MeV electron, *Nucl. Instrum. Methods Phys. Res., Sect. B*, 2017, **391**, 64–68.

22 K. Yoshizawa, H. Kato and M. Kakihana, Synthesis of Zn_2SiO_4:Mn^{2+} by homogeneous precipitation using propylene glycol-modified silane, *J. Mater. Chem.*, 2012, **22**, 17272–17277.

23 N. Taghavinia, G. Lerondel, H. Makino, A. Parisini, A. Yamamoto, T. Yao, Y. Kawazoe and T. Goto, Activation of porous silicon layers using Zn_2SiO_4: Mn^{2+} phosphor particles, *J. Lumin.*, 2002, **96**, 171–175.

24 C. Bertail, S. Maron, V. Buissette, T. Le Mercier, T. Gacoin and J.-P. Boilot, Structural and Photoluminescent Properties of Zn_2SiO_4:Mn^{2+} Nanoparticles Prepared by a Protected Annealing Process, *Chem. Mater.*, 2011, **23**, 2961–2967.

25 A. E. Morales, E. S. Mora and U. Pal, Use of diffuse reflectance spectroscopy for optical characterization of un-supported nanostructures, *Rev. Mex. Fis. S*, 2007, **53**, 18–22.

26 D. L. Wood and J. Tauc, Weak Absorption Tails in Amorphous Semiconductors, *Phys. Rev. B: Solid State*, 1972, **5**, 3144–3151.